ISSN 2543-9901

JOURNAL OF CASTING & MATERIALS ENGINEERING

QUARTERLY
Vol.4 No. 3/2020

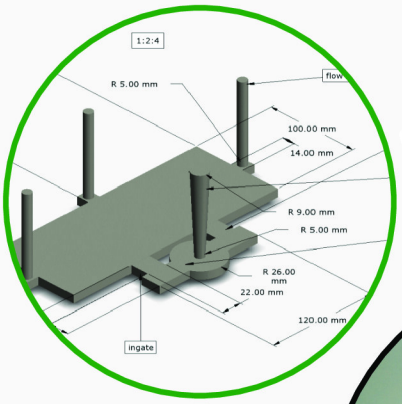

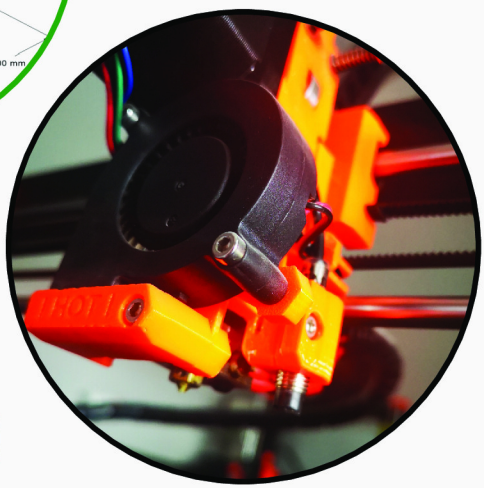

AGH UNIVERSITY OF SCIENCE AND TECHNOLOGY
FACULTY OF FOUNDRY ENGINEERING

JCME

AGH UNIVERSITY OF SCIENCE AND TECHNOLOGY PRESS KRAKOW 2020

The articles published in the Journal of Casting & Materials Engineering have been given a favorable opinion by the rewievers designated by the Editorial Board.

www:
https://journals.agh.edu.pl/jcme/

AGH UNIVERSITY OF SCIENCE AND TECHNOLOGY PRESS KRAKOW 2020

Wydawnictwa AGH (AGH University of Science and Technology Press)
al. A. Mickiewicza 30, 30-059 Kraków
tel. 12 617 32 28, 12 638 40 38
e-mail: redakcja@wydawnictwoagh.pl
http://www.wydawnictwa.agh.edu.pl

Contents

Journal of Casting & Materials Engineering Vol. 4 No. 3 (2020) 41–47
https://doi.org/10.7494/jcme.2020.4.3.41

A Statistical Analysis of Evaporative Pattern Casting Process Parameters for the Production of Aluminum Alloy Components

Babatunde Victor Omidiji*

Department of Mechanical Engineering, Obafemi Awolowo University, Ile-Ife, Nigeria
*e-mail: bvomidiji@gmail.com

Received: 12 November 2019 /Accepted: 9 July 2020/ Published online: 1 August 2020
This article is published with open access at AGH University of Science and Technology Press

Abstract

Four process parameters were investigated with the aim of determining their influence on the mechanical properties of some test castings, bars, cylinders and plates. The influence was quantified in terms of percentage contribution. Analysis of variance (ANOVA), regression, main effects and interaction effects plots were employed to carry out the statistical analysis. As regards the tensile strength of the test castings, the geometry of components (GOC) dominated, contributing 90.83% and the pouring temperature (PT) contributed 91.90% influence on the hardness property. These dominating potentials of these two parameters limited the interaction of the parameters studied in the research.

Keywords:
process parameters, analysis of variance, interaction effects, test castings and mechanical properties

1. INTRODUCTION

The evaporative pattern casting (EPC) process was developed in 1958 [1] with a distinguishing feature of evaporative patterns made of polystyrene foam (EPS) [2–5] buried in sand moulds and never removed, as is the case with traditional sand casting methods. This makes the process different from previous methods [6]. The process is known to be very sensitive to foundry parameters and variable changes [7]. Many names have been coined and given to the process, such as replicast, lost foam, full mould and evaporative process [1] but what is important is the description "evaporative'' which stands as a family name for all the trade names that have been coined so far [8, 9]. The use of loose and green sand for the lost foam process credited to Smith Flemming in 1964 and full mould process respectively as mould materials brings to the fore the subtle difference that exists in the two forms of the evaporative process [4].

The process has some advantages over other sand casting methods such as dimensional accuracy, surface finish, sand reclamation and low cost of production [2, 3]. It is believed to be environmentally friendly because the moulding material is not chemically treated [10], unlike in the other moulding methods where the moulding material is treated chemically before it is disposed after use [11]. Binders and other additives are not used. Other sand casting methods use these to bind sand grains together and improve on the properties [5]. This may have been informed by the coating applied on the surface of the patterns buried in evaporative moulds. Its disadvantages are associated with the pattern material used in the process [12].

In this work, four process parameters; pouring temperature (PT), grain fineness number (GFN), gating ratio (GR) and geometry of components (GOC) are investigated to determine their effects on the mechanical properties; tensile strength, percent elongation and the hardness of some test castings; cylinders, plates and bars. Taguchi's approach [13] to the design of experiments was employed to determine the number of experiments. This was found to be nine runs (three bars, cylinder and plates) to provide for good statistical analysis of the parameters. The coating applied on the pattern was developed from silica sand and kaolin with alcohol as the carrier.

The statistical analysis provides for the determination of the effects of the parameters on the mechanical properties. Main and interaction effects plots were made to explain these aspects. An analysis of variance tables on each of the properties are also provided. Minitab (17.0), in its trial version, was used to automatically generate the plots and tables.

2. MATERIALS AND METHODS

2.1. Materials

The materials used in the research are presented in Table 1.

Table 1
Materials used in the research

S/N	Material	Source	Uses
1	Pattern material	Polystyrene foam (EPS)	To make patterns of bars, cylinders and plates
2	Binding material	Glue	For binding the patterns and gating systems
3	Moulding material	River sand	To construct moulds
4	Casting material	Al-Si alloy	To produce the bars, cylinders and plates
5	Coating material (silica sand, kaolin and alcohol)	River sand, clay deposit, methyl alcohol	To produce the coating

Pattern material

Polystyrene material was the pattern material used in this research. It was used because it turns to gas, leaving a cavity in the mould at the point of contact with molten metal. The density value of the one employed in this research is 20 kg/m^3. It had a glassy, sparkling appearance and the ability to float on water. The water absorption capability is close to zero.

Pattern preparation

Simple shapes such as bars, cylinders and plates were selected for test castings. The dimensions of the patterns are as follows:

- bar: 250 mm × 10 mm × 10 mm,
- cylinder: Φ150 mm × H150 mm,
- plate: 250 mm × 100 mm × 10 mm.

Patterns were prepared by machining from blocks of polystyrene foam with a pre-heated wire. This was done to ensure that the surfaces of the patterns were smooth. Afterwards, the patterns were coated with refractory material. The purpose was to separate the patterns from the moulding sand and provide refractory protection to ensure no metal penetration.

Material for binding the pattern and gating system

Glue was used for binding the pattern and gating system. The glue was lightly applied to the joints of the sprue, runner bar and ingates. The glue must not be heavily applied because of its wetness so that the joints can dry within a short time. The pattern with the gating system joined together was allowed to dry at the joints before being buried in the mould. The glue employed here is white in colour, usually used for the bonding of woods in woodwork practices.

Moulding materials (green sand)

Three moulding sand samples were collected from three different sand deposits. The samples had their grain fineness numbers (GFN) as 67, 75 and 100 respectively and the values are representations of grain distribution. The GFN values were determined by sieve analysis. The moisture contents of the moulding sand samples are 3.0%, 3.4% and 4.0% respectively, while the refractoriness values are 1420°C, 1380°C and 1350°C respectively. In preparing the sand, it was turned several times for thorough mixing to produce good flowability around the mould. When thoroughness was ensured in the mixing procedure, the sand was parked around the mould and rammed to bury the pattern and the gating system. However, the pouring cup was open to the outside through which the molten metal was poured.

Casting material

An aluminum alloy casting material was used. Chemical compounds present in the Al-alloy were determined by X-ray diffractometer (XRD) model 10 monochromatic CuK α-radiation (wavelength = 1.5406 μm). The XRD of the Al-alloy is presented in Figure 1 and the elemental composition of the Al-alloy is presented in Table 2.

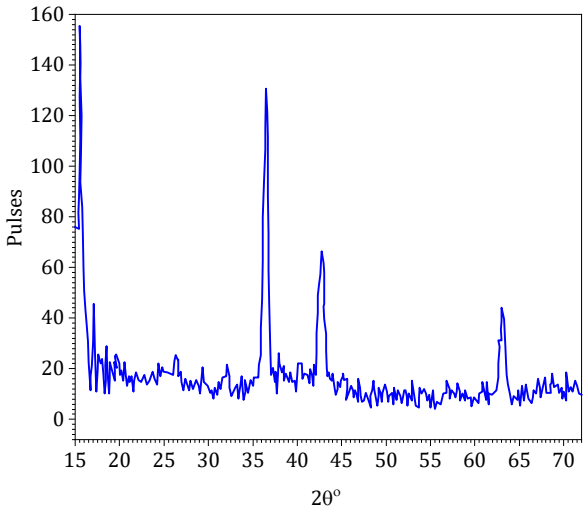

Fig. 1. XRD pattern of the Al-alloy

Table 2
Elemental composition of the Al-alloy

Element	Si	Mg	Fe	Cu	Mn	Cr
%	1.960	0.310	0.330	0.580	0.095	0.015
Element	Ni	Zn	Ti	Pb	Al	
%	0.026	0.515	0.020	0.050	96.100	

Upon investigation of the Al-alloy using XRD, it was discovered that the alloy contained aluminum silicate ($Al_2(SiO_4)O$)--orthorhombic as the highest peak and the other peaks with aluminum oxide (Al_2O_3)-monoclinic and aluminum oxide-cubic. The elemental composition and XRD were done to describe the casting material.

2.2. Methods

Mould preparation

Evaporative pattern casting process uses one flask mould, unlike the traditional sand casting process that uses two or three. There were three sand samples of different grain fineness numbers and compositions used for the sand moulds. The sand samples were taken from three different locations of sand deposits. For each run of experiment, the sand sample was packed around the pattern as designed, using Taguchi's approach. This provides for four different process parameters to be observed in a single run of the experiment. For example, for the plate cast at 650°C, the sand used as moulding material had GFN of 67, the geometry was a plate and the gating ratio was 1:2:4. As the mould was prepared, a pattern with a gating system was introduced into the mould; with the gating system consisting of the down sprue, sprue base well, runners and ingates. These were determined in calculations in the design of gating system for Al-alloys. The patterns and gating system were buried in the mould by compaction of the moulding sand in the mould. The height and width of the mould for plate and bar were 110 mm and 350 mm respectively. For the cylinder, the height of the mould was 310 mm. The projections at the sides of plate and bar castings provided for venting and flow off so that gases from the mould could escape. There were three sources of gas; molten metal, moulding material and polystyrene used as pattern material.

Melting and pouring of the molten Al-alloy

The aluminum alloy was melted in a pit furnace. Furnace fuel oil was used to fire the furnace. Alloy of about 15 kg was melted in the furnace each time that a bar, cylinder and plate were cast. Degassing was done when the alloy had melted, and just about to be poured into the prepared moulds. Hexachloromethane was employed in degassing at the pouring temperature.

The parameters observed and varied during the process of pouring included the following:

- pouring temperature: 650°C, 700°C and 750°C,
- grain fineness of moulding sand: 67, 75 and 100,
- gating ratio: 1:2:4, 1:3:3 and 1:4:4,
- geometry of components: bar, cylinder and plate.

The use of a K type (nikel-chromium) thermocouple with a grinded junction was employed to measure the temperatures. If the temperature was higher than needed, the melt was allowed to lose heat. Temperatures were taken at intervals to prevent the temperature dropping below that which was required. As soon as the desired temperature was attained, pouring was done quickly; otherwise the molten metal would solidify.

Shakeout operation and fettling of the castings

Shakeout was done after solidification of the molten metal had taken place inside the mould. Time must be given to allow solidification to take place. By using a trowel, the shakeout operation was done to carefully remove the sand packed around the pattern, gating and feeding system. After the castings were taken out of the moulds by breaking the moulds, the sand particles on the castings were removed with the use of a wire brush. This was followed by dressing, filing away the unwanted projections and the gating systems were cut off with a hacksaw. The isometric views of the test casting produced using gating ratio 1:2:4 are presented in Figures 2, 3 and 4.

Mechanical properties evaluation

Tensile test samples were taken from the castings to evaluate their mechanical properties; ultimate tensile strength (UTS), percent elongation and hardness. Instron tensile testing machine was used for the UTS and percent elongation while a microhardness tester was used to obtain the hardness values.

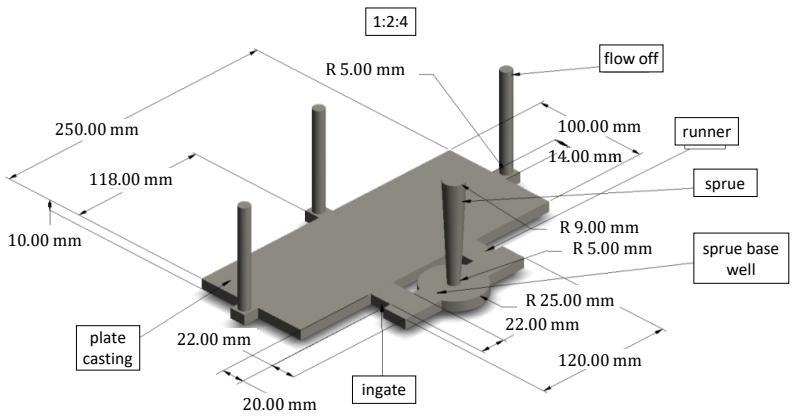

Fig. 2. An isometric view of plate casting

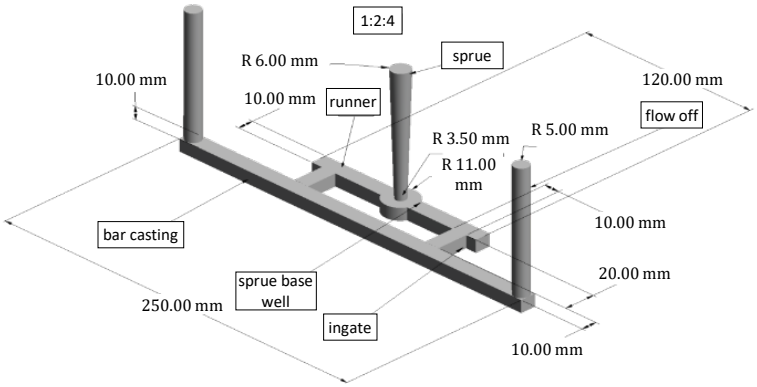

Fig. 3. Isometric view of bar casting

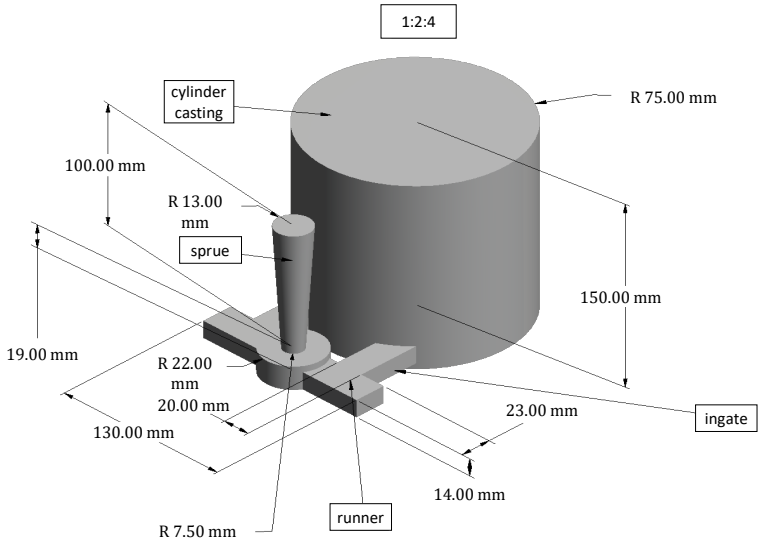

Fig. 4. Isometric view of cylinder casting

Experimental design

Using Taguchi's approach to experiment design and observing the four process parameters, nine runs of experiments were conducted. This is presented in Table 3. For each experiment, the four variables are observed at the same time.

Table 3
Taguchi's approach to design of experiments applied to EPC process

Runs of experiments	Process parameters			
	Pouring temperature (°C)	Geometry of components	Grain fineness number	Gating ratio
1	650	Plate 1	67	1:2:4
2	650	Bar 1	75	1:3:3
3	650	Cylinder 1	100	1:4:4
4	700	Plate 2	75	1:4:4
5	700	Bar 2	100	1:2:4
6	700	Cylinder 2	67	1:3:3
7	750	Plate 3	100	1:3:3
8	750	Bar 3	67	1:4:4
9	750	Cylinder 3	75	1:2:4

3. RESULTS AND DISCUSSION

The mechanical properties in terms of the ultimate tensile strength (UTS), modulus of elasticity, percent elongation and hardness of the nine castings produced are presented in Table 4. It was observed that the results decreased with the increase in pouring temperature.

Table 4
Tensile and hardness properties values of simple shape castings

Experiments	UTS (MPa)	Modulus of elasticity (MPa)	Percent elongation	Hardness (Vk)
Bar 1	147.25	12081.79	3.10	135
Bar 2	129.88	11239.05	3.04	129
Bar 3	126.14	11178.88	2.44	121
Cylinder 1	97.53	15441.23	6.07	140
Cylinder 2	89.44	14309.85	3.32	134
Cylinder 3	85.82	12903.72	2.02	124
Plate 1	143.53	11943.77	5.84	140
Plate 2	135.58	11876.06	2.55	131
Plate 3	131.22	11700.33	1.75	122

The reason adduced for this was that the structures of the castings produced with pouring temperature 650°C had fine grains, hence the greatest impediments to dislocations that needed to be overcome [4].

3.1. Analysis of results

Attempts were made to analyze the results using analysis of variance (ANOVA) for each of the properties that was measured. In the analysis, ANOVA tables, scattered, main effects and interaction plots were provided to explain the effects of the variables on the mechanical properties of the castings. Regression equations have also been provided.

3.2. Analysis on UTS

The ANOVA is presented in Table 5. From the table, it was observed that the geometry of components (GOC) had the largest contribution. From Table 5, it was observed that the cylinder had the lowest values of UTS. The reason may be attributed to its size, which prolonged the solidification time and leading to low values of the UTS.

Table 5
ANOVA for UTS

Source	DOF	Sum of squares	Mean of squares	F – values	P – values	Contribution (%)
PT (°C)	2	365.59	182.79	–	–	8.30
GOC	2	3999.13	1999.56	–	–	90.83
GFN	2	21.99	10.65	–	–	0.48
GR	2	16.70	8.35	–	–	0.38
Error	0	0.00	–	–	–	0.00
Total	8	4402.71	–	–	–	100.00

Pouring temperature contributed 8.30% and the other two parameters were insignificant in their contributions. The regression equation for the UTS shown in Equation (1) provides a way for prediction so that UTS could be predicted when values of other process parameters are put in the Equation (1).

$$\text{UTS} = 229.8542 - 0.1524\ \text{PT}\ (°\text{C}) + 0.0979\ \text{GOC} - + 0.0346\ \text{GFN} - 0.0005\ \text{GR} \quad (1)$$

where:

PT – pouring temperature,
GOC – geometry of components,
GFN – grain fineness number,
GR – gating ratio.

The scattered plot presented in Figure 5 shows the experimental and predicted values of the UTS; the predicted values are lower than the experimental ones. From Figure 5, it was observed that the UTS values of the components bars and plates were on top while those of the cylinders were at the bottom of the plots. This shows that UTS values of plates and bars are higher than the cylinder. This explains the geometry of the test castings with respect to solidification time [4, 8].

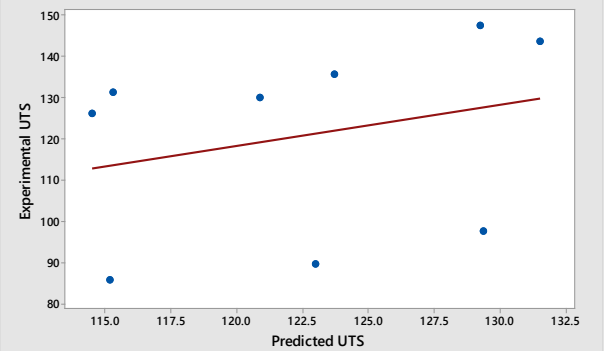

Fig. 5. Scattered plot on UTS

The main effects of the parameters on the UTS are presented in Figure 6. There are four segments in the plot, showing the variables. In each segment the variable is placed against the UTS, and reveals that pouring temperature 650°C produced the highest value of the UTS. The bars showed the highest strength amongst the components, attributed to its being slender and solidified on time. Its GFN 75 and gating ratio 1:3:3 produced the best ultimate tensile strength.

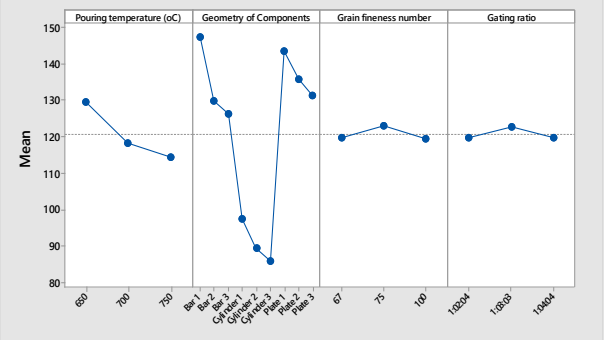

Fig. 6. Main effect of variables on UTS

The interaction effect of the variables on the UTS of the castings is presented in Figure 7. The values of the UTS obtained experimentally are placed on the *y*-axis and those quantities of the variables are on the *x*-axis. The plot is of four divisions; pouring temperature, geometry of components, grain fineness number and gating ratios. The effects of the interactions of pouring temperature and GFN, pouring temperature and gating ratio and GFN and gating ratio on UTS were investigated. From Figure 7, it was discovered that interaction between these variables were not very well pronounced. However, the plots depict the real behavior of the variables other than the main one shown in Figure 6. For example, a gating ratio of 1:3:3 was shown to be predominant in Figure 6 but coming to Figure 7, in the third column and fourth row, two points were dominant while the third point was at the bottom. The plot shows that pouring temperature has an effect on the first column fand row, geometry of components has effects on the second column and row, GFN has effects on the third column and row and gating ratio has effects on the fourth column and row. Looking at the interaction between the gating ratio and GFN, it is discovered that the gating ratio of 1:3:3 was dominant. Next to it was the gating ratio of 1:2:4.

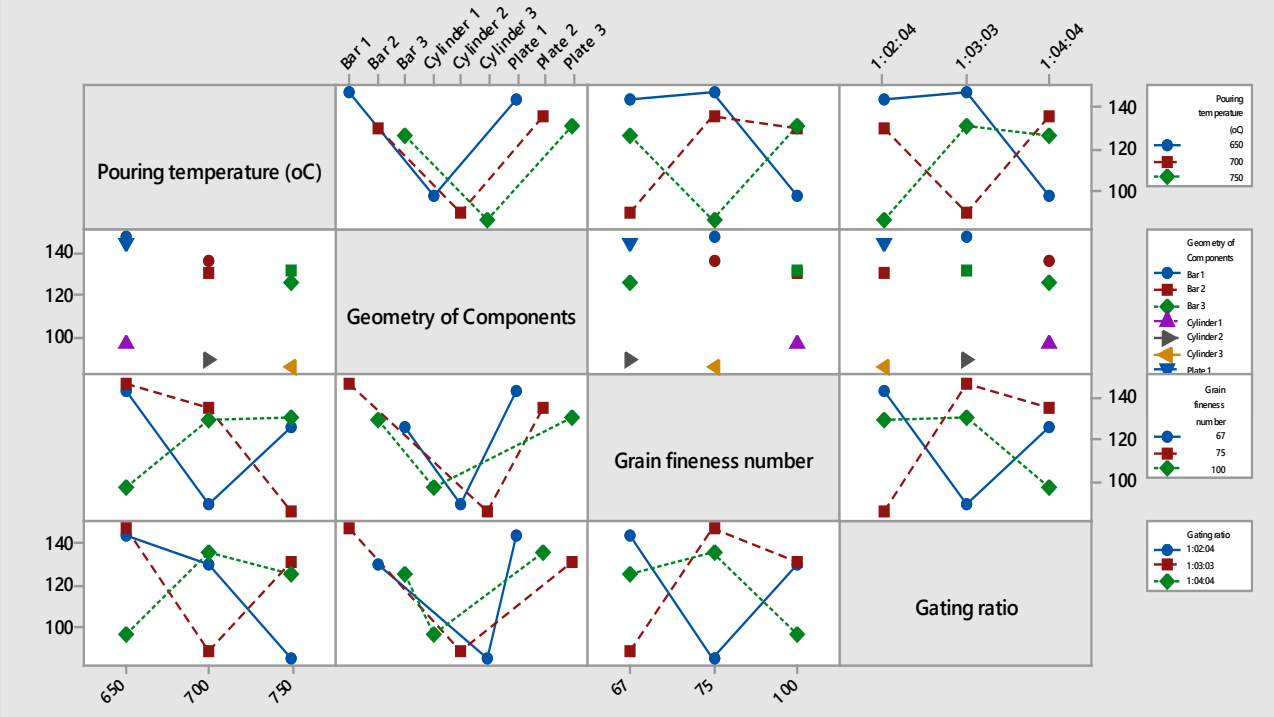

Fig. 7. Interaction effects of variables on UTS

3.3. Analysis on hardness

The hardness values of the test castings had been presented in Table 4 and the analysis of variance is presented in Table 6. From Table 6, it is observed that pouring temperature played a dominant role on the hardness of the test castings, contributing 91%. The geometry of components is about 7% contribution and the last two variables are insignificant in contribution.

Table 6
ANOVA for Hardness

Source	DOF	Sum of squares	Mean of squares	F – values	P – values	Contribution (%)
PT (°C)	2	386.000	193.000	–	–	91.90
GOC	2	28.667	14.333	–	–	6.83
GFN	2	4.667	2.333	–	–	1.11
GR	2	0.667	0.333	–	–	0.16
Error	0	0.000	–	–	–	0.00
Total	8	420.000	–	–	–	100.00

The regression equation for the hardness of the test castings is given in Equation (2).

$$\text{Hardness} = 255.4449 - 0.1626\ \text{PT (°C)} + 0.1310\ \text{GOC} - + 0.0261\ \text{GFN} - 0.0031\ \text{GR} \quad (2)$$

The Equation (2) is significant in predicting what the values of hardness would be suppose the parameters are changed and different values are put into the equation. The scattered, main effect and interaction effect plots are shown in Figures 8, 9 and 10 respectively.

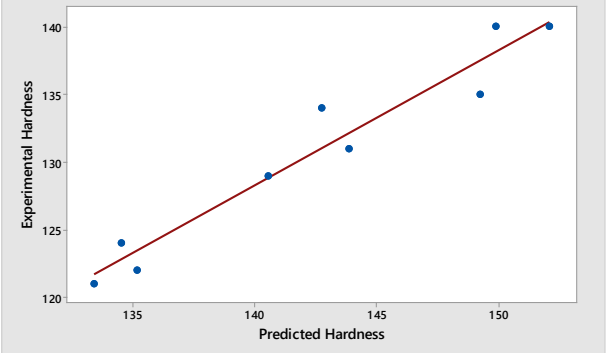

Fig. 8. Scattered plot for hardness

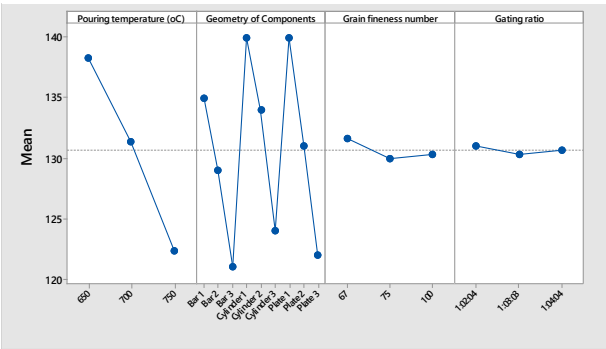

Fig. 9. Main effects for hardness

In Figure 8, the experimental and predicted values of the hardness are shown. It is observed that the predicted values are higher than the experimental ones. From Figure 9, a pouring temperature of 650°C produced the highest value of hardness cylinder 1, grain fineness number of 67 and a gating ratio of 1:2:4 produced the highest value of hardness.

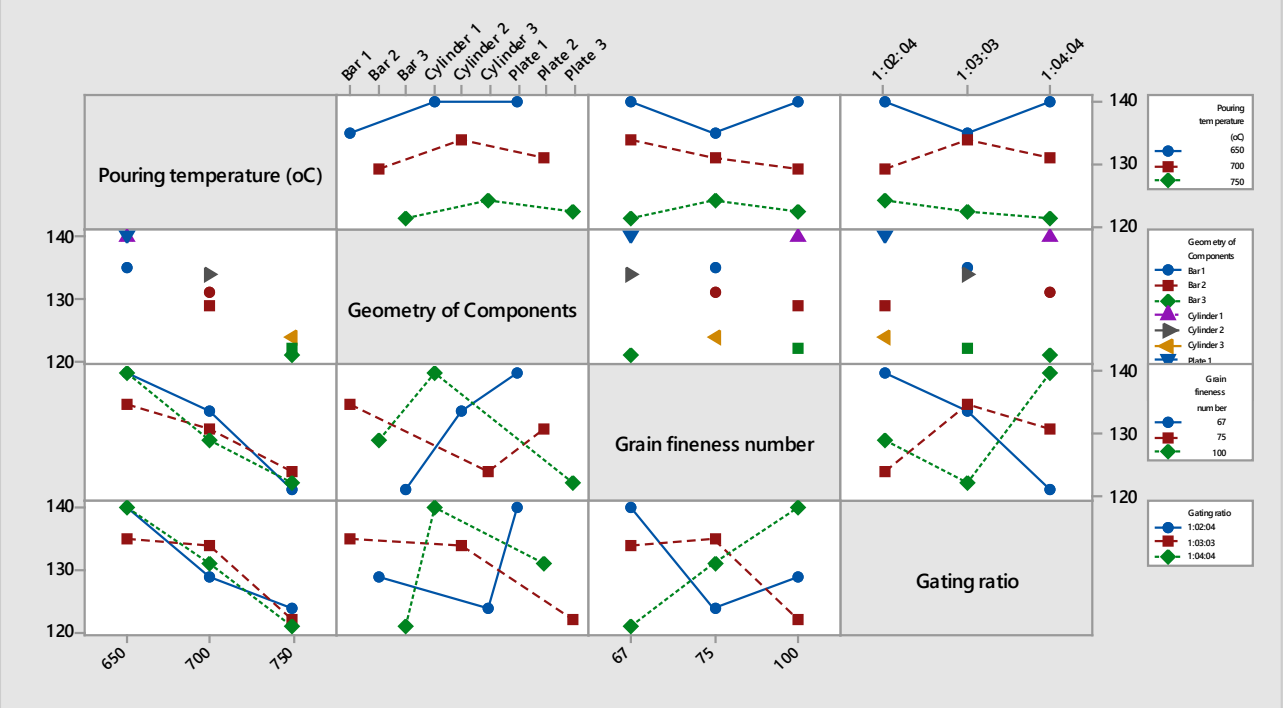

Fig. 10. Interaction effects for hardness

Figure 10 gives the interaction effects of the parameters on the hardness. The Figure is in four segments; pouring temperature, geometry of components, grain fineness number and gating ratio. From Table 6, it is observed that pouring temperature is dominant, contributing over 90% of influence, which also shows in Figure 9 where pouring temperature is dominant throughout in interaction with other process parameters.

4. CONCLUSION

Regression equations for the UTS and the hardness properties of the test castings, bar, cylinders and plates were formulated, which are good for prediction by substituting variable values that were not used in this research. The ANOVA showed the contribution of each of the parameters investigated. It had been observed that the dominating potential of pouring temperature in the case of the hardness values and geometry of components as regards the UTS reduced the interaction tendency of the parameters. However, the influence of each of the parameters in terms of percent contribution was shown.

REFERENCES

[1] Clegg A.J. (1991). *Precision Casting Processes*. Oxford (England), New York: Pergamon Press Plc.

[2] Kumar S., Kumar P. & Shan H.S. (2006). Parametric optimization of surface roughness castings produced by Evaporative Pattern Casting Process. *Materials Letters*, 60, 3048–3053.

[3] Kumar S., Kumar P. & Shan H.S. (2007). Effects of evaporative pattern casting process parameters on the surface roughness of Al-7%Si alloy castings. *Journal of Materials Processing Technology*, 182, 615–623. Doi: 10.1016/j.jmatprotec.2006.09.005.

[4] Kumar S., Kumar P. & Shan H.S. (2008). Optimization of tensile properties of evaporative pattern casting process through Taguchi's method. *Journal of Materials Processing Technology*, 204, 59–69. Doi: 10.1016/j.jmatprotec.2007.10.075.

[5] Kumar S., Kumar P. & Shan H.S. (2009). Characterization of the refractory coating material used in vacuum assisted evaporative pattern casting process. *Journal of Materials Processing Technology*, 209, 2699–2706.

[6] Houzeaux G. & Codina R. (2004). A finite element model for the simulation of lost foam casting. *International Journal of Numerical Methods in Fluids*, 46, 203–226. Doi: 10.1002/fld.757.

[7] Liu X.J., Bhavnani S.H. & Overfelt R.A. (2007). Simulation of EPS foam decomposition in the lost foam casting process. *Journal of Materials Processing Technology*, 182, 333–342.

[8] Omidiji B.V. (2014). *Evaporative pattern casting (EPC) process for production of Aluminum Alloy Components* [Ph.D Thesis]. Federal University of Technology, Minna.

[9] Omidiji B.V. (2018). *Evaporative pattern casting (EPC) process.* Advanced Casting Technologies. Intechopen.

[10] Behm S.U., Gunter K.L. & Sutherland J.W. (2003). *An investigation into the effect of process parameter settings on air characteristics in the lost foam casting process*. Michigan Technological University, Houghton, Michigan.

[11] Kannan P., Biernacki J.J. & Visco D.P. (2007). A review of physical and kinetic models of thermal degradation of expanded polystyrene foam and their application to the lost foam casting process. *Journal Analytical Application of Pyrolysis*, 78, 162–171.

[12] Liu J., Ramsay C.W. & Askeland D.R. (1996). A Study of Foam-Metal-Coating Interaction in the LFC Process. *Transactions of the American Foundrymen's Society*, 105, 419–425.

[13] Yadav N. & Karunakar D.B. (2011). Effects of Process Parameters on Mechanical Properties of the Investment Castings Produced by Using Expandable Polystyrene Pattern. *International Journal of Advances in Engineering and Technology*, 1 (3), 9–18.

Journal of Casting & Materials Engineering Vol. 4 No. 3 (2020) 48–52
https://doi.org/10.7494/jcme.2020.4.3.48

Polylactide Used as Filment in 3D Printing – Part 1: FTIR, DRIFT and TG-DTG Studies

Beata Grabowska*, Karolina Kaczmarska, Sylwia Cukrowicz, Elżbieta Mączka, Artur Bobrowski

AGH University of Science and Technology, Faculty of Foundry Engineering, Reymonta 23, 30-059 Krakow, Poland
e-mail: beata.grabowska@agh.edu.pl

Received: 5 August 2020 /Accepted: 9 September 2020 /Published online: 30 September 2020
This article is published with open access at AGH University of Science and Technology Journals

Abstract

A short literature review was undertaken in terms of the structure, properties and applications of polymers, including those commonly used in 3D printing. The research part included the structural and thermal analysis of polylactide (PLA), which is an example of an extensively used polymer in the developing 3D technology. Special attention was paid to the comparison of structure and thermal stability of two different (from various producers) polylactide samples. The research, involving such analytical methods as infrared spectroscopy (FTIR) and diffuse reflectance infrared spectroscopy (DRIFT), allowed the comparison of the structure of the two PLA samples considered. The determination of the temperature range in which changes related to PLA thermodestruction occur was a result of the performed thermoanalytical research (DRIFT, TG-DTG). Thermal studies also allowed to establish the temperature range in which the material does not yet degrade, which is important in the context of future planned research work on polylactide modification to obtain the improvement of the thermal and mechanical properties of PLA-based materials. This research area will be described in the second part of the publication.

Keywords:

polylactide, 3D printing technology, thermal degradation, FTIR, TG-DTG

1. INTRODUCTION

3D printing technology is focused on the fabrication of wax patterns followed by final products being obtained in the lost wax casting process. It is especially useful in the production of small parts and assemblies used in miniaturized electronic devices and also in toy and jewellery manufacturing. Biomedical equipment, such as biocompatible implants, dental prosthetics, orthodontics and orthopedics are the most common medical applications of the 3D printing technique (Fig. 1) [1–10].

At present, a wide spectrum of materials is used for additive manufacturing in 3D printing technology. Their selection is closely related to the application of the achieved model/prototype. Contemporary materials mostly include polymers but also metals and ceramics.

While creating an illustrative visualization of the 3D planning models, cheap materials are considered, e.g. polyethylene (PE), acrylonitrile butadiene styrene (ABS) of technical purity. However, for the production of individualized elements intended to be introduced into the human body, biomaterials that meet specified requirements are needed. Biocompatibility, non-toxicity, and hypoallergenic properties are key to the successful application of implant materials. Biodegradable polymers such as polylactide (PLA), polyglycolide (PGA), poly(lactide-*co*-glycolide) (PLGA), polycaprolactone (PCL) belonging to the group of synthetic polymers, polydimethylsiloxane (PDMS), being the simplest member of the silicone polymer family, and chitin, chitosan, collagen of natural polymers are used with considerable degrees of success [11, 12].

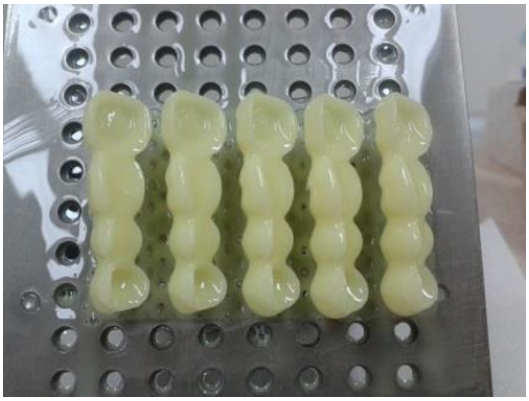

Fig. 1. 3D printed cast patterns of dental bridges [3]

Polylactide [poly(lactic acid), PLA] belongs to the group of aliphatic polyesters (Fig. 2). The synthesis of PLA can be performed by the direct polycondensation of lactic acid or by the ring-opening polymerization of lactide (LA). LA possesses two chiral centers and can thus exist in three distinct diastereoisomers, namely, DD-, LL-, and DL-. Therefore, PLA shows stereochemical diversity. Depending on the synthesis conditions three forms of PLA with different properties can be obtained: poly(L-lactide) (PLLA), poly(DL-lactide) (PDLLA), and poly(D-lactide) (PDLA) [11, 12].

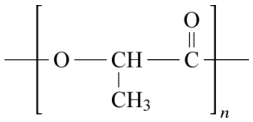

Fig. 2. Structure of polylactide

In general, PLA is a transparent thermoplastic polymer, quite stiff and brittle, and at the same time completely biodegradable. The disadvantage of PLA is its water absorption tendency, resulting from the presence of ester groups in its structure. The effect is greater with more amorphous polymer. However, the properties of PLA strongly depend on the composition of the repeat units (L and D) and their distribution along the polyester chain. PLA is not soluble in water, but it is soluble in dichloromethane (DCM) and dimethylformamide (DMF). The degradation rate of PLA depends on many factors, among the most important of which are: the molecular weight and the stereochemical composition, the type of end groups, the shape and the thermal history, the temperature and pH of the environment. In the first stage, the hydrolytic degradation (reverse process to condensation) with a decrease in the molecular weight of PLA occurs. The second stage is biological degradation under the influence of microorganisms that break down PLA oligomers into water and CO_2. The time of PLA hydrolytic degradation in an inert environment at 37°C ranges from several months to 1 year. However, for the meso-polylactide form, biodegradation lasts up to several weeks. The great majority of the manufacturing and processing of PLA is carried out at 200°C, ensuring a melt viscosity of less than 10^3 Pa·s. Under these conditions, PLA quite easily undergoes hydrolytic degradation and depolymerization processes. Ester bond breaking reactions are also possible [11, 12].

The high cost of the PLA synthesis limits its wider use, since the large-scale production of polylactide is too expensive for applications in the packaging industry [4, 5, 7]. Therefore, it is most often directed towards medical purposes as a material for the controlled drug release. Bioresorbable implants and surgical sutures, clamps, clips, surgical masks, dressings, compresses, medical staff clothing, pharmaceutical products and personal care materials are the main areas for PLA medical applications [8–10]. The great advantage of poly(lactic acid) and its copolymers results from the fact that its degradation products are natural metabolites. There is growing research interest in PLA, focused on reducing its production cost in order to expand the range of its applications, particularly in the packaging industry and the production of alternative fibers to nylon [4, 12]. Although polylactide-based materials have been commonly processed into medical products by conventional techniques (e.g., casting, porogen leaching), PLA, its copolymers and composites are also increasingly often used in 3D printing technology [13, 14]. Breast-shaped poly(D,L)-lactide scaffolds fabricated by the melt extrusion were investigated for their potential in the long-term sustained regeneration of adipose tissue [15]. Poly-L-lactide copolymers such as poly(L-lactide-*co*-ε-caprolactone) and poly(L-lactide-*co*-glycolide) were considered as tubes for absorbable nerve guides and scaffolds for bone tissue engineering [16, 17]. Different additive manufacturing (AM) technologies were used: solution extrusion and selective laser sintering, respectively.

The publication is an introduction to the wider research plan on the modification of polylactide in the context of its use as a filament in 3D printing technology. As a starting point, the structural and thermoanalytical analysis of two commercial filaments commonly used in the 3D printing technique was assumed. The determination of the temperature range in which PLA does not degrade is important in the context of the planned research work on its modification to improve the thermal and mechanical properties of PLA-based materials. The planned modification is aimed at a specific type of 3D printer dedicated to the production of detailed components for the automotive industry. The next part of the publication will present the research results on the resulting filament containing PLA.

2. EXPERIMENTAL

2.1. Materials

Two commercial polylactide (PLA) filaments from different sources were tested: 1 – blue (INK3.DE) and 2 – black (VAKIND). The PLA-based samples were parts of polymers rolls of circular cross-section measuring 1.75 mm in diameter.

2.2. Thermogravimetric analysis (TG-DTG)

Thermal analysis was performed using a Jota thermal analyzer. The examinations were carried out in open platinum crucibles using a sample mass ca. 10 mg under an oxidizing atmosphere (synthetic air) (flow rate 40 ml/min) and in the temperature range from 25°C to1000°C. The heating rate of the test sample was 10°C/min.

2.3. Structural analysis by the transmission technique (FTIR)

The structural tests were performed using the transmission technique (with KBr pellets) with the use of a Digilab Excalibur FTS 3000 Mx spectrometer with the DTGS detector. The sample preparation for the FTIR technique required making pellets (ϕ10 mm). To receive them, the materials had to be finely ground to produce particles that were smaller than the wavelength of IR radiation (5 μm). Then, the prepared PLA-based samples in the amount of 2 mg were mixed with 200 mg of powdered, pure and dry potassium bromide (KBr). The pellets obtained by

compressing the mixtures in a hydraulic press at 200 bar for 1 min were then placed in the measuring chamber of the spectrometer. The obtained spectrum of each sample was compared with the background spectrum (KBr). The spectrum was recorded by the Varian Resolution Pro program, within an infrared radiation range of 4000–400 cm^{-1}, with a power of resolution of 4 cm^{-1}. The interferograms consisted of 32 sample scans, which were averaged over one spectrum.

2.4. Thermal analysis by diffuse reflectance technique (DRIFT)

Diffuse reflectance technique for infrared analysis of PLA samples was performed by means of an attachment connected to the devices for temperature and water cooling system control. The temperature spectra was recorded in the range of 25–400°C in the wavenumber range of 4000–600 cm^{-1} with the set resolution of 8 cm^{-1}. The interferograms consisted of 64 sample scans, which were averaged over one spectrum.

The infrared beam was focused by a series of mirrors on the surface of the sample, which was placed in a sample holder. Diffuse radiation through the powder was collected by other mirrors and sent to the detector. Preparation of the samples included grinding the tested materials in an agate mortar and mixing them with powdered KBr in an empirically selected proportion. The sample holder, a ceramic crucible, was placed inside a dome with zinc selenium (ZnSe) windows. As the infrared beam penetrates only the top 0.5–2.0 mm of the material, the lower half of the crucible was filled with pure KBr powder.

The data were registered under the conditions of increasing temperature in the atmosphere of oxygen. The recording of the spectra began 1 min after the pre-determined temperature was reached. The normalization of the spectra was performed by way of comparing the obtained spectrum with the background spectrum (KBr).

3. RESULTS AND DISCUSSION

3.1. TG-DTG analysis

Figure 3 shows the TG-DTG results for polylactide samples. Thermal decomposition of both PLA1 sample (Fig. 3a) and PLA2 sample (Fig. 3b) started at the same moment (after reaching the temperature of 300°C). The difference in the TG-DTG curves of the tested polymers indicates on better thermal stability of the PLA1 sample. Its thermal degradation occurred in the temperature range of 300–500°C. The final weight loss was 99.03%. The changes, under the influence of temperature, appeared more rapidly in the PLA2 sample. The polymer decomposition ended at 400°C. Its weight loss was 99.29%, so it was higher than the final PLA1 mass loss by 0.26%. It can also be seen that between 300°C and 400°C the PLA1 TG curve is non-linear. Therefore, the nature of its degradation process is slightly more complex than the thermal decomposition of the second polymer (PLA2).

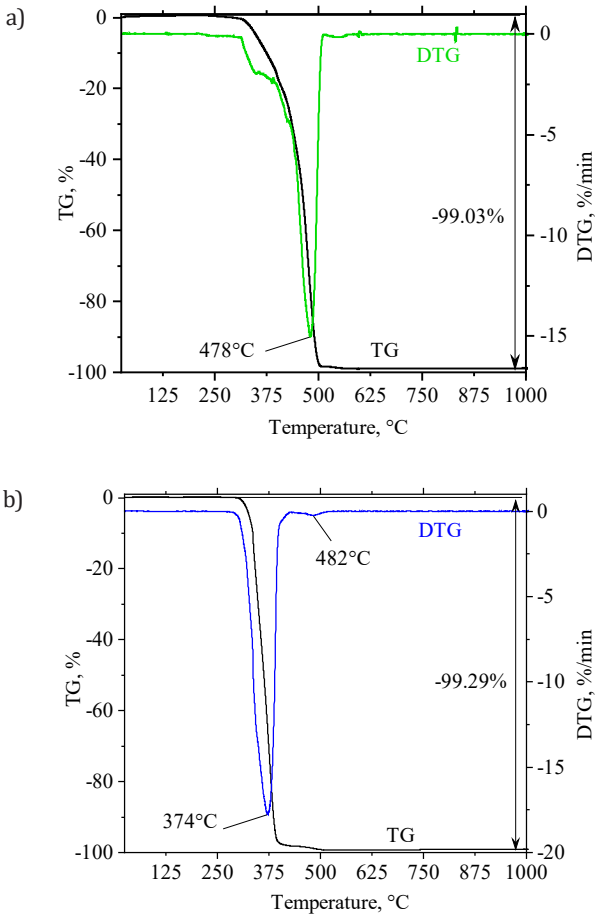

Fig. 3. TG-DTG curves of: a) PLA1; b) PLA 2

3.2. Structural analysis

FTIR spectra of PLA samples have been shown in Figure 4.

The absorption bands of low intensity in the wavenumber region of about 3500 cm^{-1} are typical of the free O–H group (H_2O). The maxima of the bands at 2925 cm^{-1}, 2848 cm^{-1} (spectrum 1) and 2998 cm^{-1}, 2945 cm^{-1} (spectrum 2) are assigned to C–H stretching vibrations.

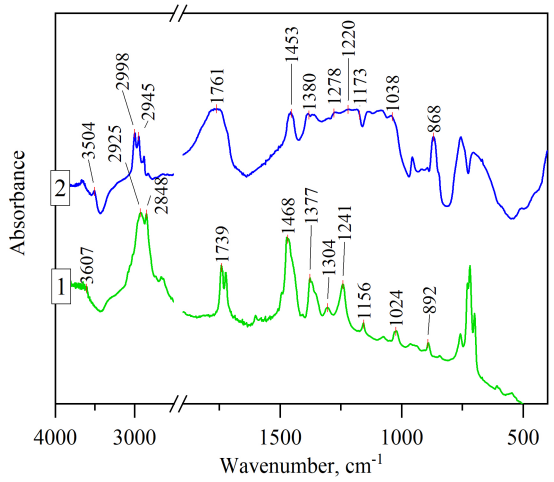

Fig. 4. IR spectra of: 1) PLA1; 2) PLA2

Characteristic bands of polylacite functional groups can also be distinguished. The absorption bands observed in the range of wavenumber 1739–1761 cm^{-1} and 1156–1173 cm^{-1} correspond respectively to the stretching vibrations of C=O and C–O–C groups. The noticeable differences in the bands related to, e.g., C=O bending vibrations (1220 cm^{-1} on spectrum 1 and 1241 cm^{-1} on spectrum 2), which can be seen in both spectra, may be the result of the presence of additives (dyes) in the samples.

Identified bands on IR spectra for a PLA samples are summarized in Table 1.

Table 1
Characteristic absorption bands on the IR spectra of PLA samples

Sample		Assignment	Remarks
PLA1	PLA2		
Wavenumber, cm^{-1}			
3504	3607	ν-OH	Band of free OH group (water)
2998	2925	ν-C–H $\nu(CH_2)$	Stretching vibrations asymmetric and symmetric
2945	2848		
1761	1739	ν_s-C=O	Stretching vibrations of carbonyl group
1453	1468	$\beta(CH_3)$	In-plane bending vibrations
1380	1377	δ-CH–	Deformation vibrations asymmetric and symmetric
1278	1304		
1220	1241	–C=O	Bending vibrations
1173	1156	ν-C–O–	Stretching vibrations
1038	1024	ν-OH	Stretching vibrations
868	892	–C–C	Stretching vibrations

Figure 5 depicts the DRIFT temperature spectra obtained for the polylactide samples.

The determination of the structural changes occurring in PLA1 (Fig. 5a) and PLA2 (Fig. 5b) was carried out under the conditions of increasing temperature in the range of 25–500°C. The DRIFT spectra were recorded in the middle infrared range of 4000–600 cm^{-1} by the technique of diffuse reflectance spectroscopy. In both spectra, the shape and position of the bands changes as the temperature increases. The intensity of certain bands also changes, some disappear completely. Moreover, new bands appear.

The characteristic peaks appearing on the DRIFT spectra in a region of low wavelength of the PLA1 sample (Fig. 5a) are: the C–O–C deformation vibrations which correspond to peaks at 730 and 928 cm^{-1} and the C–C stretching vibrations at 1057 cm^{-1}. The bands with maxima wavenumbers of 1361 and 1445 cm^{-1} can be attributed to CH_3 (deformation) groups, while at 2924 cm^{-1} to CH_3 (stretching) groups. The new band at 1584 cm^{-1} is assigned to ester group (COO). The sharp, strong peak at 1762 cm^{-1} corresponds to C=O vibrations. There is also a small OH peak at 3713 cm^{-1}.

The changes in PLA1 structure (Fig. 5a) that appear with increasing temperature are mainly related to its progressive thermal degradation. Above 300°C, in the wavelength range from 730 to 1584 cm^{-1}, a gradual increase in the band intensity can be observed, especially in the area at 1240 cm^{-1}. A similar tendency can be noticed in the case of bands with peaks at 1762 and 2924 cm^{-1}. In these areas, the bands extension was also registered. At the same time (at the temperature of 300–400°C), a new band appears with a maximum at 1584 cm^{-1}, which can be attributed to $\nu_{as}(OCO)$ vibrations. This may indicate the formation of gaseous products, i.e. mixtures of carbon dioxide and oxygen gases.

The course of structural changes of PLA2 (Fig. 5b) is similar, except that shifts of maximum bands are observed and visible changes in the intensity of some bands are observed (increase in intensity at 400°C with a maximum of 1765 cm^{-1}, 1093 cm^{-1}). Bands not present in the DRIFT spectra of PLA1 have also been observed – with a maximum of 1190 cm^{-1} and 864 cm^{-1}, which are likely to be associated with different additives (e.g. dyes) in the filament.

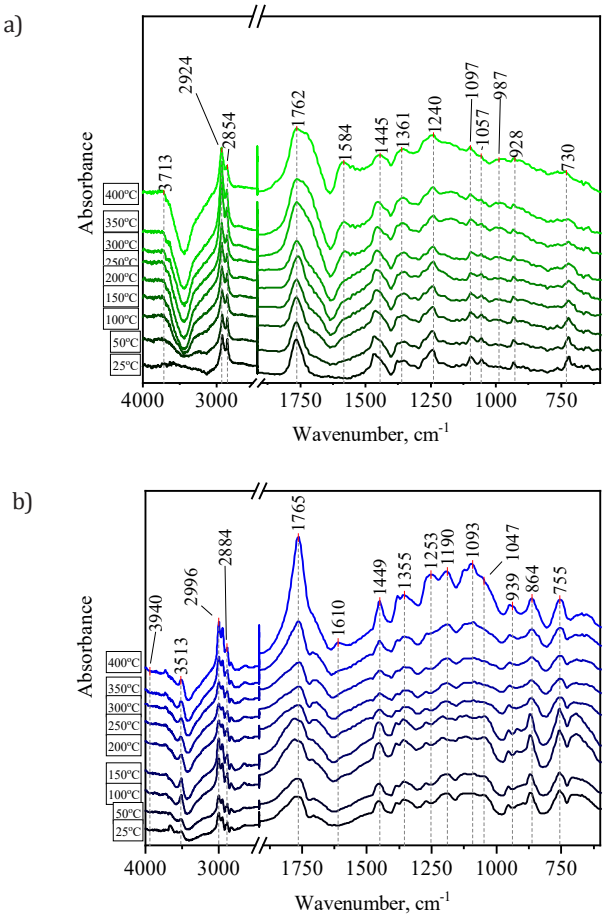

Fig. 5. DRIFT spectra recorded for the a) PLA1; b) PLA2 sample in the temperature range of 25–400°C

4. CONCLUSIONS

The complex thermoanalytical analysis (FTIR, DRIFT, TG-DTG) allowed the determination of the temperature range in which the initial commercially available polylactide does not undergo thermal degradation but only reversible transformations, and thus does not lose its functional properties.

On the basis of the obtained test results, it can be stated that both PLA samples are thermally stable in the temperature range 25–300°C. Thus, the operating temperature of a typical 3D printer where the processing of polylactide takes place, is not exceeded (*extrusion temperature* is not exceeded). In addition, the information obtained is important in terms of optimizing the conditions of its processing, including the use of 3D printing technology for the production of details for the automotive industry.

REFERENCES

[1] Kaziunas France A. (2014). *Świat druku 3D. Przewodnik*. Gliwice: Wydawnictwo Helion.

[2] Dodziuk H. (2019). *Druk 3D/AM. Zastosowania oraz skutki społeczne i gospodarcze*. Warszawa: Wydawnictwo Naukowe PWN.

[3] Dikova T., Dzhendov D., Bliznakova K. & Ivanov D. (2016). Application of 3D printing in manufacturing of cast patterns. *VIIth International Metallurgical Congress*, 9–12 June 2016, Ohrid, Macedonia.

[4] Manas C. & Salil R. (2008). *Industrial polymers, specialty polymers and their applications*. Boca Raton, USA: CRC Press.

[5] Syrek H. (2013). Zastosowanie drukarek 3D do wytwarzania modeli woskowych w procesie odlewania metodą traconego wosku. *Nafta-Gaz*, 69(12), 929–935.

[6] Przybytek A., Kucińska-Lipka J. & Janik H. (2016). Thermoplastic elastomer filaments and their application in 3D printing. *Elastomery*, 20(4), 32–39.

[7] Sasimowski E. (2015). Przyrostowe metody wytwarzania elementów z tworzyw polimerowych. *Przetwórstwo Tworzyw*, 21(4), 349–354.

[8] Sarecka-Hujar B., Ostróżka-Cieślik A. & Banyś A. (2016). Innowacyjne technologie w medycynie i farmacji. *Acta Bio-Optica et Informatica Medica. Inżynieria Biomedyczna*, 22(1), 9–17.

[9] Lee V., Singh G., Trasatti J.P., Bjornsson C., Xu X., Tran T.N., Yoo S.S., Dai G. & Karande P. (2014). Design and fabrication of human skin by three-dimensional bioprinting. *Tissue Engineering: Part C: Methods*, 20(6), 473–484. Doi: 10.1089/ten.TEC.2013.0335.

[10] Kusaka M., Sugimoto M., Fukami N., Sasaki H., Takenaka M., Anraku T., Ito T., Kenmochi T., Shiroki R. & Hoshinga K. (2015). Initial experience with a tailor-made simulation and navigation program using a 3-D printer model of kidney transplantation surgery. *Transplantation Proceedings*, 47(3), 596–599. Doi: 10.1016/j.transproceed.2014.12.045.

[11] Florjańczyk Z. & Penczek S. (1995). *Chemia polimerów*, Vol. 1: *Makrocząsteczki i metody ich otrzymywania*. Warszawa: Oficyna Wydawnicza Politechniki Warszawskiej.

[12] Rabek J.F. (2008). *Współczesna wiedza o polimerach*. Warszawa: Wydawnictwo Naukowe PWN.

[13] Woźna A. (2012). Struktura kompozytów bioresorbowalnych wytworzonych z zastosowaniem generatywnej metody laserowej. *Modelowanie Inżynierskie*, 14(45), 134–138.

[14] Poh P.S.P., Chhaya M.P., Wunner F.M., De-Juan-Pardo E.M., Schilling A.F., Schantz J.T., van Griensven M. & Hutmacher D.W. (2016). Polylactides in additive biomanufacturing. *Advanced Drug Delivery Reviews*, 107, 228–246.

[15] Chhaya M.P., Melchels F.P.W., Holzapfel B.M., Baldwin J.G. & Hutmacher D.W. (2015). Sustained regeneration of high-volume adipose tissue for breast reconstruction using computer aided design and biomanufacturing. *Biomaterials*, 52, 551–560.

[16] Thapsukhon B., Thadavirul N., Supaphol P., Meepowpan P., Molloy R. & Punyodom W. (2013). Effects of copolymer microstructure on the properties of electrospun poly(L-lactide-*co*-ε-caprolactone) absorbable nerve guide tubes. *Journal of Applied Polymer Science*, 130(6), 4357–4366.

[17] Simpson R.L., Wiria F.E., Amis A.A., Chua C.K., Leong K.F., Hansen U.N., Chandrasekaran M. & Lee M.W. (2008). Development of a 95/5 poly(L-lactide-*co*-glycolide)/hydroxylapatite and β-tricalcium phosphate scaffold as bone replacement material via selective laser sintering. *Journal of Biomedical Materials Research Part B: Applied Biomaterials*, 84B(1), 17–25.